Local Lattice Distortion in the Giant Negative Thermal Expansion Material $Mn_3Cu_{1-x}Ge_xN$

S. Iikubo,[1] K. Kodama,[1] K. Takenaka,[2,3] H. Takagi,[3,4] M. Takigawa,[5] and S. Shamoto[1]

[1]*Quantum Beam Science Directorate, Japan Atomic Energy Agency, Tokai, Ibaraki, 319-1195, Japan*
[2]*Department of Crystalline Materials Science, Nagoya University, Nagoya, Aichi, 464-8603, Japan*
[3]*RIKEN (The Institute of Physical and Chemical Research), Wako, Saitama, 351-0198, Japan*
[4]*CREST, Japan Science and Technology Agency, Kawaguchi, Saitama, 332-0012, Japan*
[5]*Institute for Solid State Physics, University of Tokyo, Kashiwa, Chiba, 277-8581, Japan*

(Received 1 May 2008; revised manuscript received 27 August 2008; published 14 November 2008)

Giant negative thermal expansion is achieved in antiperovskite manganese nitrides when the sharp volume change associated with magnetic ordering is broadened by substitution. In this Letter, we address the unique role of the ''magic'' element, Ge, for such broadening in $Mn_3Cu_{1-x}Ge_xN$. We present evidence for a local lattice distortion well described by the low-temperature tetragonal (T_4) structure of Mn_3GeN for a range of x, where the overall structure remains cubic. This structural instability shows a strong correlation with the broadness of the growth of the ordered magnetic moment and, hence, is considered to trigger the broadening of the volume change.

DOI: 10.1103/PhysRevLett.101.205901 PACS numbers: 65.40.De, 61.05.F−, 75.25.+z, 75.80.+q

Negative thermal expansion (NTE) materials, which enable fine control of thermal expansion, have significant technological importance because even a variation of the linear thermal expansion coefficient α, as small as one part in 10^6, crucially degrades the performance of devices in many precise applications [1–3]. The recent development of ''metallic'' antiperovskite nitrides Mn_3AN [4–6] showing giant negative thermal expansion, where A is a metal or a semiconducting element [7,8], has promoted research toward practical use. The NTE occurs as a result of the volume expansion accompanied by magnetic ordering, the so-called magnetovolume effect (MVE). We pointed out the intimate relationship between the large MVE in cubic Mn_3AN and the Γ^{5g}-type antiferromagnetic (AF) ordering [9]. The importance of the magnetic structure has not been considered in the conventional theory of MVE [10].

The technological essence of NTE in Mn_3AN is the discovery of Ge and Sn dopants that broaden the volume change. In $Mn_3Cu_{1-x}Ge_xN$, a sharp MVE appears at $x \sim 0.15$. Around $x = 0.5$, a gradual change of the lattice parameter gives rise to a large negative slope in the linear thermal expansion over a wide temperature (T) range [4–6]. Clarifying the mechanism for the broadening of the MVE (the Invar problem) has been a challenge in solid state physics over a century. But now it appears to be understood as due to the gradual increase of the local magnetic moment and the resultant volume expansion [10–15]. The clarification of the broadening mechanism of MVE also provide us a useful guideline for designing NTE materials with better performance and other applications utilizing the first-order magnetic phase transition [16]. The strong preference of Ge and Sn for broadening the MVE in Mn_3AN revealed in previous studies [4–6] indicates importance of the atomic and/or chemical characteristic of dopants. Therefore, it is crucial to obtain local information. This is a novel aspect beyond the conventional concepts proposed for other itinerant electron systems.

In this study, we have performed neutron powder diffraction and NMR measurements on $Mn_3Cu_{1-x}Ge_xN$ to obtain local magnetic and structural information. For the magnetic part, we confirmed that the amplitude of the ordered moment grows in a wider T range with increasing Ge doping. For the lattice part, we found that the local lattice distortion described by the alternating rotation of the Mn_6N octahedra around the c axis appears for a range of x, where the average structure remains cubic. Such distortion, which becomes more significant as the Ge doping proceeds, is what has been observed in the low-temperature tetragonal (T_4) structure of Mn_3GeN. This strongly suggests that the instability between the cubic and the T_4 structures induced by Ge substitution is related to the broadening of MVE.

The measurements have been done on powder samples of $Mn_3Cu_{1-x}Ge_xN$ with $x \geq 0.15$. The compounds at $x \sim 0$ show magnetic ordering accompanied by cubic (C: space group $Pm\bar{3}m$) to tetragonal ($P4/mmm$) structural transition without MVE [5]. The compounds in the range $0.15 \leq x \leq 0.7$ show Γ^{5g}-type AF ordering, maintaining a cubic crystal structure in the whole T range, and exhibits a large MVE [9]. For $x \sim 1$, the systems shows magnetic ordering with successive structural phase transitions, reaching the tetragonal T_4 ($I4/mcm$) structure at the lowest temperature ($T < 510$ K) [7,17], but do not exhibit MVE. As a reference, the neutron diffraction experiment has been performed also on Mn_3GaN. This material shows a first-order magnetic transition at $T = 290$ K with Γ^{5g} AF ordering accompanied by a large MVE but the structure remains cubic down to low temperatures. Sample preparation and characterization have been described elsewhere [4–6,8].

Neutron diffraction experiments were performed using the high-resolution powder diffractometer HRPD(λ = 1.8233 Å) and the triple axis spectrometer TAS-2(λ = 2.3590 Å) installed at JRR-3 of JAEA. Time-of flight neutron diffraction measurement was performed using the NPDF instrument at the Los Alamos Neutron Science Center (LANSCE). The NMR spectra of ^{14}N were measured by integrating the spin-echo intensity in a swept magnetic field at 19.90 MHz.

Figure 1(a) shows the T dependence of the (100) magnetic reflections of $Mn_3Cu_{1-x}Ge_xN$ for $x = 0.15$, 0.5, and 0.7, and of Mn_3GaN, where the intensities are normalized by the (110) nuclear reflection. The (100) reflection has large intensity in the Γ^{5g} AF magnetic structure. The magnetic reflection intensity grows in a progressively wider T range with increasing Ge content. The width of the magnetic peaks are nearly resolution limited, suggesting long-range Neel ordering. Figure 1(b) shows the T dependence of the width of the field-swept ^{14}N-NMR spectra for $x = 0.4$ ($T_N \sim 300$ K) displayed in the inset. The line width increases gradually with decreasing T in the ordered state [18]. Since the NMR line width represents the average value of the magnetic hyperfine field from the ordered moment, the gradual change of the line width indicates the gradual growth of the magnitude of the AF ordered moments, consistent with the neutron result. Details of the neutron diffraction and the NMR experiments will be described separately [19].

Because the splitting of the nuclear Bragg peak is not observed below the magnetic ordering temperature, these magnetic transitions occur without breaking the cubic symmetry. The inset of Fig. 1 shows the lattice parameters obtained from neutron diffraction patterns using the simple cubic model at various temperatures. The T dependence of lattice constant is consistent with the linear thermal expansion reported in Ref. [4]. Based on the neutron and the NMR results, we conclude that the systems with a gradual volume change exhibit a gradual change in the magnitude of the ordered moments.

Although the overall crystal structure remains cubic for $0.15 < x < 0.7$ in the whole T region, interestingly, the atomic pair distribution function (PDF) shows considerable deviation of the local structure in short length from the average cubic structure. The PDF technique yields local structural information [20–22] contrary to the Rietveld refinements that gives the long-range structure. The experimental PDF $G(r)$ is obtained from the total scattering structure function $S(Q)$ in the range of $1.8 < Q < 30$ Å^{-1} via the Fourier transformation using the PDFgetN program [23]. The calculated PDF is obtained using the PDFFIT program [24].

We first examine the experimental PDF obtained for $Mn_3Cu_{0.5}Ge_{0.5}N$ at 300 K using cubic structure model. Figure 2 displays the result of fitting in the range of $1.5 < r < 10$ Å, where the red line indicates the calculated PDF. In this model, all atomic positions are fixed. We refined scale factor, lattice constant, occupancy parameters, isotropic thermal factors, and broadening parameters from the sample. For small amounts of MnO impurities (~3%), scale factor, lattice constant, and isotropic thermal factors are refined. The overall experimental PDF up to 10 Å is well reproduced by the cubic structure. For example, the

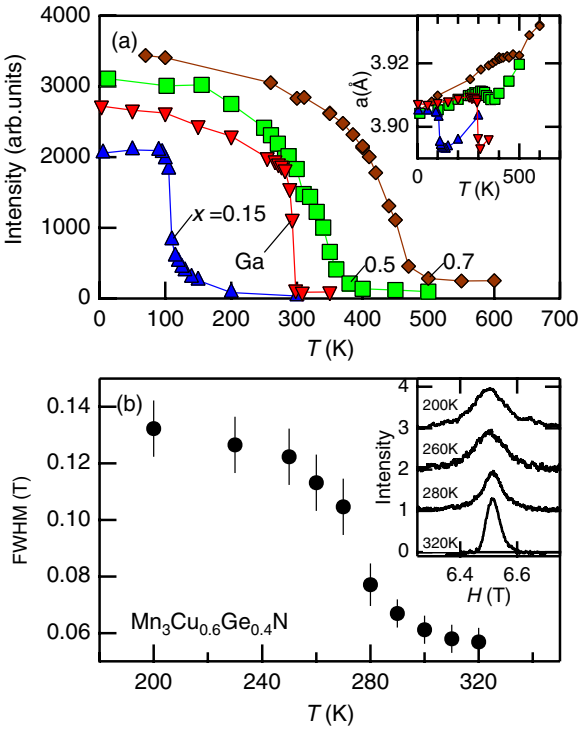

FIG. 1 (color online). (a) T dependence of the magnetic reflection intensity of $Mn_3Cu_{1-x}Ge_xN$ and Mn_3GaN. The inset shows the T dependence of lattice constants. (b) FWHM of ^{14}N-NMR spectra on $Mn_3Cu_{0.6}Ge_{0.4}N$ as a function of temperature. The inset shows the field-swept ^{14}N-NMR spectra at several temperatures.

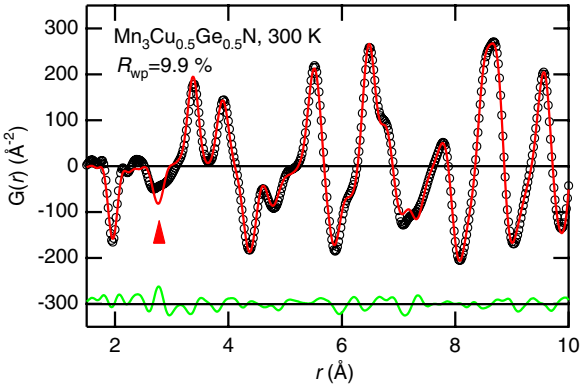

FIG. 2 (color online). PDF fit of the neutron scattering for $Mn_3Cu_{0.5}Ge_{0.5}N$. Circles correspond to the experimental PDF, and the fit with cubic model is the red line through the data. The difference curve is shown at the bottom. A large difference is observed in the second-nearest peak indicated by a closed triangle.

obtained lattice parameter of 3.9100(4) is consistent to the value of 3.9113(8) in the diffraction pattern. On the other hand, we notice a marked difference in the short length. The observed width of the second negative peak at around 2.8 Å is much wider than the calculated one. Because the second peak comes from the positive Mn-Mn contribution within the Mn_6N octahedra and negative Mn-Cu (or Ge) contribution, the large width is attributed to the latter contribution. The Mn-Mn and Mn-Cu (or Ge) bonds are shown in Fig. 3(a) as thick red and thin black lines, respectively. In the ideal cubic structure, the second peak should be as sharp as the first peak at ~1.9 Å, because the bond lengths are identical. The first peak, which comes from the Mn-N correlation in Mn_6N octahedra, is well reproduced by the cubic structure. The observed PDF provides clear evidence for the local distortion on the Mn-Cu (or Ge) correlation against relatively rigid Mn-N bonds.

The distribution of the Mn-Cu (or Ge) bond length is related to the low-temperature tetragonal structure of Mn_3GeN. Mn_3GeN shows a transition from the high T cubic to the low T tetragonal T_4 ($I4/mcm$) phase at $T_t \sim$ 540 K [17,25]. The transition primarily involves alternate rotations of the Mn_6N octahedra around the z axis shown in Fig. 3(b), resulting in an enlarged unit cell with $\sqrt{2}a \times \sqrt{2}a \times 2c$ [17,25]. There are three different Mn-Ge bond lengths denoted by L, M, and S. The experimental PDF of Mn_3GeN at $T = 330$ K is displayed in Fig. 4(a). Among the three negative peaks at ~1.9 Å, ~2.6 Å, and ~3.1 Å, the first peak is attributed to the Mn-N bond, where the relative large width is due to the distortion of Mn_6N octahedra in the T_4 phase. The second and third peaks are explained by the two Mn-Ge bond lengths denoted by S and L. The negative contribution of the almost invariant M bond (~ 2.8 Å) is canceled by the positive contribution of the Mn-Mn correlation. We performed T_4 model fit to the experimental PDF in the range $1.5 < r < 5$ Å, and displays the data up to 3.5 Å. The T_4 model have additional fitting parameters, atomic position of Mn ion occupying $8h$ (u, $u + 1/2$, 0) relating to the rotation of the octahedra and tetragonal lattice parameters. The peak structure is well reproduced by the calculation with $u = 0.195(5)$ in the T_4 model, where the C model is described by $u = 0.25$.

The anomalous broadening of the second peak (~2.8 Å) observed for $x = 0.5$ can be also explained by the rotation of Mn_6N octahedra. We show the the result fitting in the range of $1.5 < r < 5$ Å at room temperature for $Mn_3Cu_{0.85}Ge_{0.15}N$, $Mn_3Cu_{0.5}Ge_{0.5}N$, and Mn_3GaN in Figs. 4(a)–4(d), respectively. Each R_{wp}s shown in the figures are lower than the values obtained in the C model, $R_{wp} = 10.2$, 14.2, and 10.9%, respectively. Obtained u parameters are 0.240(2), 0.232(1), and 0.240(2), respectively. Although these systems have an average cubic structure, the sharp first peak (~1.9 Å) and the broad second peak (~2.8 Å), are well reproduced by the calculation for the T_4 model shown by the lines.

Furthermore the splitting of the second peak, denoted by the tickmarks in the figure show the systematic x dependence. At $x = 0.15$, the negative peak at around 2.8 Å has a double-peak structure. A similar double-peak structure but with wider splitting is observed at $x = 0.5$. The peak splitting of the second negative peak increases with x but the width of the first peak remains unchanged. These results indicates that the local crystal structure of $Mn_3Cu_{1-x}Ge_xN$ approaches the structure of Mn_3GeN with increasing Ge content.

From the structure refinement with the T_4 model in short length, we found that the rotation angle θ of Mn_6N octahedra, which is shown in Fig. 3(b), is a good indicator of the broadening of the MVE. From the refined u

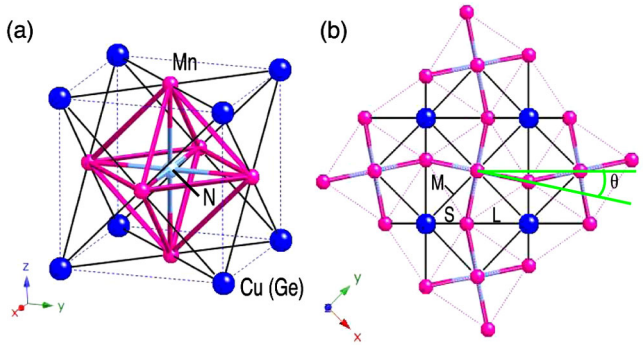

FIG. 3 (color online). (a) Cubic crystal structure of antiperovskite. (b) The tetragonal T_4 crystal structure viewed from the z axis. Alternate rotation of Mn_6N octahedra occurs along the z axis. The three different Mn-Cu(Ge) bonds are denoted by thin solid black lines labeled L, M, and S. The octahedral rotation angle is denoted by θ. Note that the tetragonal cell has lattice vectors in the a-b plane that are the diagonals of the cubic cell.

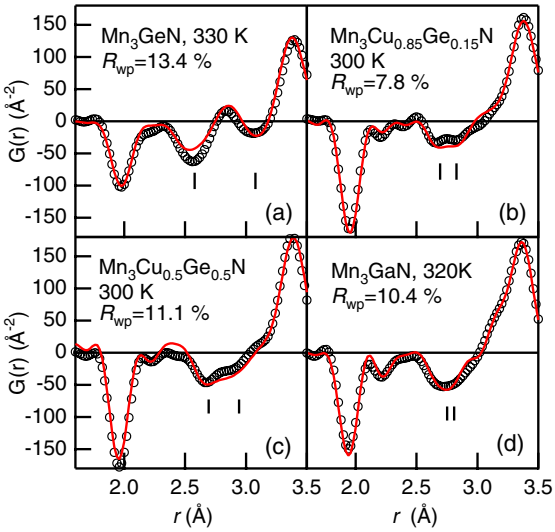

FIG. 4 (color online). Experimental PDFs (open circles) and calculated PDFs (lines) with T_4 model structure for Mn_3GeN at 330 K, $Mn_3Cu_{0.85}Ge_{0.15}N$ at 300 K, $Mn_3Cu_{0.5}Ge_{0.5}N$ at 300 K, and Mn_3GaN at 320 K. Ticks show the width of the peak splitting of Mn-Cu (or Ge) correlation.

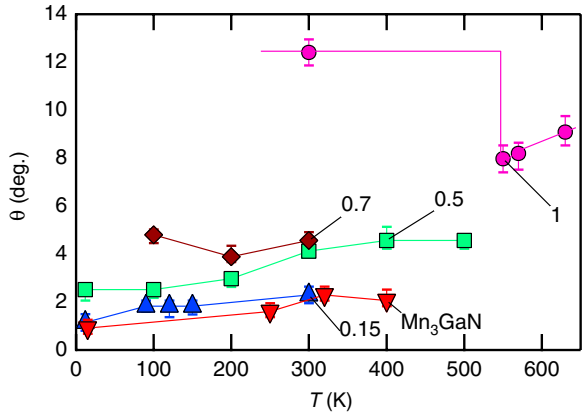

FIG. 5 (color online). Fitting results of rotation angle θ of $Mn_3Cu_{1-x}Ge_xN$ and Mn_3GaN. The line at $x = 1$ is a visual guide.

value, we estimated θ at each T, shown in Fig. 5. In $Mn_3Cu_{1-x}Ge_xN$, θ systematically increases with increasing Ge doping level x. Around room temperature, the θs are in order of $2.3(3)(Mn_3GaN) \sim 2.3(3)(x = 0.15) < 4.1(2)(x = 0.5) < 4.6(3)(x = 0.7)$. The former two samples show the sharp increase of the ordered moment at ordering temperature with decreasing T, while latter two samples show the gradual increase. Even in Mn_3GeN, the amplitude of ordered magnetic moment gradually increases with decreasing T (not shown), although the system does not show MVE [7,17]. The local octahedral rotation angle clearly correlates with the T dependence of the ordered magnetic moment.

By focusing on the local crystal structure, we found a clear signature of the structural instability between the C and T_4 phases, which has been overlooked from spatially averaged information. There is an independent experimental indication of local distortion based on XAFS studies [26]. The local structure and dynamics around doped Ge change in NTE T region. Our rotation angle θ may be the average of spatially distributed rotation angle. Structural instability seems to lead to the instability of the amplitude of magnetic moment. For the Invar alloy system, the Invar effect or an instability of the amplitude of magnetic moment also appears near the phase boundary between the fcc and bcc phases [27]. So far, the variation of magnetic phase transition has been discussed on the basis of the spatially averaged information. The present study provides the first experimental result emphasizing the importance of the local structure to the related Invar problem.

In conclusion, we found that a local T_4 structure in average cubic phase appears as Ge substitution proceeds. This strongly suggests that the gradual growth of magnetic moment leading to the broadening of MVE is related to the structural instability between C and T_4 induced by Ge substitution.

We are grateful to J. Matsuno and T. Egami for helpful discussions. The authors thank N. Igawa, M. Matsuda, and Th. Proffen for their help in the neutron diffraction measurement. This work was performed under the NIMS-RIKEN-JAEA Cooperative Research Program on Quantum Beam Science and Technology. This work has benefited from the use of NPDF at the Lujan Center at Los Alamos Neutron Science Center. Los Alamos National Laboratory is funded by DOE under Contact No. W-7405-ENG-36. This work was partly supported by NEDO, Japan.

[1] A. W. Sleight, Inorg. Chem. **37**, 2854 (1998).
[2] J. S. O. Evans, J. Chem. Soc. Dalton Trans. (**1999**) 3317.
[3] G. D. Barrera *et al.*, J. Phys. Condens. Matter **17**, R217 (2005).
[4] K. Takenaka and H. Takagi, Appl. Phys. Lett. **87**, 261902 (2005).
[5] K. Takenaka and H. Takagi, Mater. Trans., JIM **47**, 471 (2006).
[6] K. Takenaka *et al.*, Appl. Phys. Lett. **92**, 011927 (2008).
[7] D. Fruchart and E. F. Bertaut, J. Phys. Soc. Jpn. **44**, 781 (1978).
[8] T. Kaneko *et al.*, J. Phys. Soc. Jpn. **56**, 4047 (1987).
[9] S. Iikubo *et al.*, Phys. Rev. B **77**, 020409(R) (2008).
[10] T. Moriya and K. Usami, Solid State Commun. **34**, 95 (1980).
[11] P. Mohn *et al.*, Phys. Rev. B **43**, 3318 (1991).
[12] Mark van Schilfgaarde *et al.*, Nature (London) **400**, 46 (1999).
[13] Y. Takahashi and H. Nakano, J. Phys. Condens. Matter **18**, 521 (2006).
[14] Y. Kakehashi, Physica (Amsterdam) **161B**, 143 (1989).
[15] M. Shiga and Y. Nakamura, J. Phys. Soc. Jpn. **47**, 1446 (1979).
[16] First-order magnetic phase transition attracts much attention in terms of its potential for magnetic refrigeration technology. See, for example, T. Tohei *et al.*, J. Appl. Phys. **94**, 1800 (2003); A. Fujita *et al.*, Phys. Rev. B **65**, 014410 (2001).
[17] M. Barberon *et al.*, Mater. Res. Bull. **5**, 1 (1970).
[18] In the Γ^{5g} AF cubic phase, the hyperfine field induced by ordered Mn moments is perfectly cancelled at N site. However, because of the local distortion (shown by PDF), the finite contribution remains.
[19] K. Kodama *et al.* (to be published).
[20] T. Egami and S. J. L. Billinge, *Underneath the Bragg Peaks: Structural Analysis of Complex Materials* (Pergamon, Elsevier, 2003).
[21] X. Qiu *et al.*, Phys. Rev. Lett. **94**, 177203 (2005).
[22] K. Kodama *et al.*, J. Phys. Soc. Jpn. **76**, 124605 (2007).
[23] P. F. Peterson *et al.*, J. Appl. Crystallogr. **33**, 1192 (2000).
[24] Th. Proffen and S. J. L. Billinge, J. Appl. Crystallogr. **32**, 572 (1999).
[25] Although the appearance of the successive phase transition in Mn_3GeN depends on sample preparation condition, the structure at the lowest temperature ($T < 510$ K) is the identical T_4 structure. See Ref. [17].
[26] J. Matsuno (private communication).
[27] E. F. Wasserman, *Ferromagnetic Materials*, edited by K. H. J. Bushow and E. P. Wohlfarth (Elsevier Science Publishers, New York, 1990), Vol. 5, p. 237.